DOI: 10.1002/chem.200700783

Platinum Phenanthroimidazole Complexes as G-Quadruplex DNA Selective Binders

Roxanne Kieltyka, Johans Fakhoury, Nicolas Moitessier, and Hanadi F. Sleiman*[a]

Abstract: Complexes that bind and stabilize G-quadruplex DNA structures are of significant interest due to their potential to inhibit telomerase and halt tumor cell proliferation. We here report the synthesis of the first Pt^{II} G-quadruplex selective molecules, containing π-extended phenanthroimidazole ligands. Binding studies of these complexes with duplex and quadruplex $d(T_4G_4T_4)_4$ DNA were performed. Intercalation to duplex DNA was established through UV/Vis titration, CD spectroscopy, and thermal denaturation studies. Significantly stronger binding affinity of these phenanthroimidazole Pt^{II} complexes to G-quadruplex DNA was observed by UV/Vis spectroscopy and competitive equilibrium dialysis studies. Observed binding constants to quadruplex DNA were nearly two orders of magnitude greater than for duplex DNA. Circular dichroism studies show that an increase in π-surface leads to a significant increase in the thermal stability of the Pt^{II}/quadruplex DNA complex. The match in the π-surface of these phenanthroimidazole Pt^{II} complexes with quadruplex DNA was further substantiated by molecular modeling studies. Numerous favorable π-stacking interactions with the large aromatic surface of the intermolecular G-quadruplex, and unforeseen hydrogen bonds between the ancillary ethylenediamine ligands and the quadruplex phosphate backbone are predicted. Thus, both biological and computational studies suggest that coupling the square-planar geometry of Pt^{II} with π-extended ligands results in a simple and modular method to create effective G-quadruplex selective binders, which can be readily optimized for use in telomerase-based antitumor therapy.

Keywords: DNA binders · G-quadruplex · intercalations · molecular modeling · phenanthroimidazole · platinum

Introduction

The targeting of key processes encountered in both cellular ageing diseases and cancer may rest in telomeres found at the end of eukaryotic chromosomes. Telomeres are non-coding, highly repetitive sequences, typically 10–15kb in humans, which are adjacent to more gene-rich sub-telomeric regions.[1] The structure of the telomere is essentially double-stranded, except at its 3′-terminus where it exists as a long single strand composed mostly of guanine bases. It is believed that this G-rich portion of the telomere folds into a quadruplex DNA structure,[2] where four guanine bases are held in the same plane by a Hoogsteen hydrogen bond array (Scheme 1).[3,4] The function of the telomere is to protect the ends of chromosomes from base pair loss and end-to-end fusions that are encountered in replication events.[5] In somatic cells, telomeres suffer from an "end replication problem" where DNA polymerase cannot fully replicate the ends of the chromosome and thus, several bases of telomeric DNA are lost with each cell division. Eventually, the length of the telomere is rendered insufficient, signaling the cell to enter senescence then apoptosis. However, in cancer cells, short telomeres are maintained by the reverse transcriptase enzyme telomerase. Telomerase adds bases to the 3′-single stranded overhang of the telomere such as to prevent the critical shortening resulting from normal replication events, leading to the immortalization of the cancer cell. Interestingly, telomerase is not active in somatic cells, however it has shown elevated levels of expression in 85–90% of cancerous cells.[6] As a result of this discovery, a significant amount of research has been devoted to therapeutic antitumor strategies through telomerase inhibition.[7–9]

A promising strategy involves the inhibition of telomerase at the level of the telomere, as telomerase extends the telomere through the addition of bases at the 3′-terminus. It has been previously demonstrated that if the 3′-terminus of the

[a] R. Kieltyka, J. Fakhoury, Dr. N. Moitessier, Dr. H. F. Sleiman
Department of Chemistry, McGill University
801 Sherbrooke St. W., Montreal, QC, H3A 2K6 (Canada)
Fax: (+1) 514-398-2382
E-mail: hanadi.sleiman@mcgill.ca

Supporting information for this article is available on the WWW under http://www.chemeurj.org/ or from the author.

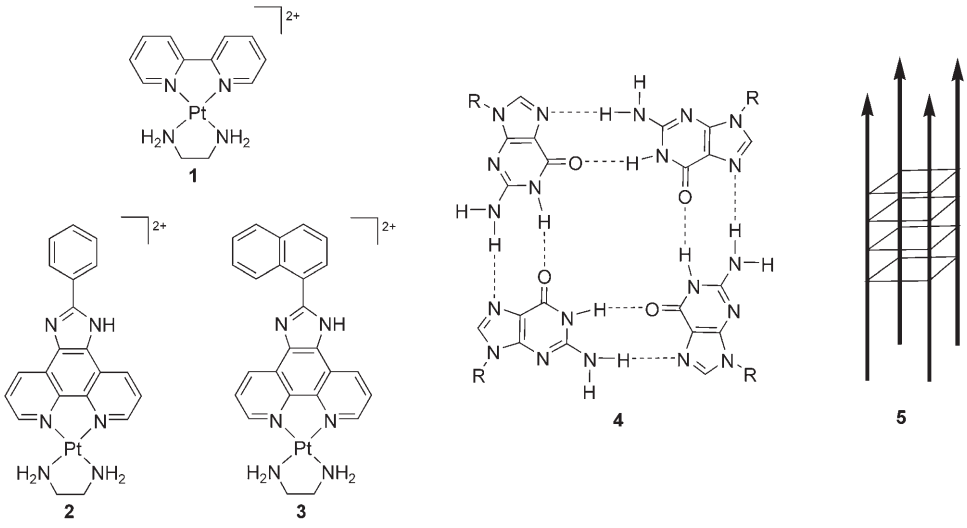

Scheme 1. Bipyridine ethylenediamine platinum(II) (**1**), phenylphenanthroimidazole ethylenediamine platinum(II) (**2**), naphthylphenanthroimidazole ethylenediamine platinum(II) (**3**), structure of guanine quadruplex (**4**), schematic of intermolecular quadruplex $d(T_4G_4T_4)_4$ (**5**)

telomere is sequestered by telomere binding proteins,[10,11] telomerase is unable to add bases,[12] thus preventing the tumor cell's immortalization. Moreover, small molecules which assist in the formation of guanine quadruplexes, or sequester pre-existing ones through strong binding affinity have been observed to halt telomerase activity. Thus, G-quadruplex binding molecules have recently emerged as a new class of potentially selective antitumor therapeutics.[13–15]

In general, an effective G-quadruplex binder possesses a large electron deficient π-aromatic surface, positively charged substituents that can interact with the grooves of the quadruplex, as well as a positively charged center which can reside near the center of the guanine quartet.[16–18] Many elegant studies on organic G-quadruplex binders have appeared,[19–21] but examples involving inorganic complexes are rare. Thus far, inorganic G-quadruplex binders have included copper,[22] manganese,[23] and nickel porphyrins,[24,25] nickel salens,[18] and ruthenium bis-intercalating complexes[26] in their design. Transition-metal complexes are extremely appealing as they introduce a myriad of geometries that are unattainable for carbon, thus expanding the existing organic G-quadruplex binder toolbox. Furthermore, these metal-based binders present an opportunity for modular and facile synthesis of compound libraries, in contrast to their organic counterparts, which often require time-consuming multistep syntheses. Through simple modifications of their coordination environment and the potential to alter their geometries, the incorporation of transition-metals into G-quadruplex binders offers unique possibilities to enhance binding affinity and selectivity for this DNA motif.

Platinum-intercalating complexes have been extensively investigated in binding studies with duplex DNA.[27,28] Previously, binding constants on the order of $10^6\,M^{-1}$ were reported for a relatively small π-surface complex, [Pt(4,4′-diphenyl-2,2′-bipyridyl)(ethylenediamine)]$^{2+}$ with duplex DNA.[29] However, for more π-extended complexes, such as [Pt(dipyridophenazine)(ethylenediamine)]$^{2+}$, surprisingly lower binding constants, on the order of $10^4\,M^{-1}$ were reported.[27] These binding constants are markedly lower than those observed for octahedral ruthenium complexes possessing the same intercalating ligand ($\approx 10^6$–$10^7\,M^{-1}$),[30] which is not as "π-extended" as the square-planar Pt^{II} complexes. This lowered affinity points to a likely size mismatch between the large π-surface of square-planar Pt^{II} complexes with extended aromatic ligands and the smaller π-surface of duplex DNA (in addition to other possible factors such as self-aggregation and electronic character).[31]

On the other hand, G-quadruplex DNA structures present a planar π-extended system that is greater in size than the duplex DNA base-pairs. We were therefore interested in exploring whether Pt^{II} complexes containing extended π-surfaces would be better suited for binding to these structures. We here report the synthesis of the first Pt^{II} G-quadruplex selective binding complexes **2** and **3**, with readily tunable phenanthroimidazole ligands. UV/Vis, circular dichroism, thermal denaturation, continuous variation analysis, and competitive dialysis experiments show that increasing the size of the π-surface in these complexes indeed leads to an increase in binding affinity and selectivity for G-quadruplexes over duplex DNA structures. This result is supported by molecular modeling studies, which in addition show end-stacking of the complexes in an "off-center" location above the G-tetrad, and stabilization by hydrogen bonding of the ethylenediamine ligand to the phosphate backbone. Overall, this study shows that combining the square-planar geometry of Pt^{II} with extended aromatic ligands can result in a simple method to access effective G-quadruplex selective binders in a few synthetic steps. The modular and facile synthesis of the phenanthroimidazole Pt^{II} scaffold is readily amenable to library creation, and further binding optimization for use in telomerase-based antitumor therapy.

Results and Discussion

Synthesis and characterization: The design of the Pt^{II} intercalating complexes includes a phenanthroimidazole ligand, which can be readily tuned by varying the substituent at the imidazole carbon atom. Phenyl and naphthyl moieties in complexes **2** and **3** were used to observe if increased binding

can be achieved through a more hydrophobic and extended π-surface (Scheme 1). The phenyl- and naphthyl-derivatized phenanthroimidazole ligands were synthesized by the condensation of 1,10-phenanthroline-5,6-dione with the aromatic (phenyl or naphthyl) aldehyde.[35] These ligands were allowed to react with potassium tetrachloroplatinate to give [Pt(phenanthroimidazole)Cl_2], followed by treatment with ethylenediamine, resulting in complexes **2** and **3**. For comparison, $[Pt(bpy)(en)]^{2+}$ (**1**), which has been previously shown to bind to duplex DNA by intercalation through a significantly less extended π-system than **2** and **3** was also synthesized and studied.

UV/Vis absorption spectra of complexes **2** and **3** and their respective ligands were recorded prior to the addition of calf-thymus DNA in a 3% DMSO/phosphate buffer solution. UV/Vis spectra for complex **2** showed a strong absorption at 279 nm, a shoulder at 305 nm, and a weak absorption at 400 nm. Both peaks at 279 nm and 305 nm are correlated with a ligand-centered π–π* transition, and the weak absorption at 400 nm is assigned to a Pt^{II} dπ–π* metal-to-ligand charge transfer band (MLCT). Complex **3** showed a strong absorbance at 253 nm and a peak at 302 nm, which are assigned to a ligand-centered π–π*, as well as a weak transition at 401 nm correlated with a Pt^{II} dπ–π* MLCT band (see the Supporting Information). UV/Vis spectra of the phenyl and naphthyl ligands of complexes **2** and **3** showed features similar to those of the complexes, with the exception of the MLCT transitions. Fluorescence spectra were measured for complex **3** and its naphthyl ligand.[36] A weak fluorescence at 417 nm was observed for the naphthyl ligand upon excitation at 330 nm, and weak fluorescence was observed as well for complex **3** under the same conditions.[37]

Duplex binding studies: DNA binding studies were conducted with the hexafluorophosphate salts of complex **2** and **3**. Molar extinction coefficients of complexes **2** and **3** to be used in the DNA binding experiments were calculated, using the shoulders at 305 nm and 302 nm, respectively (Table 1).

Table 1. Molar extinction coefficients of Pt^{II} complexes, spectral shifts and binding affinity with the addition of calf-thymus DNA.

Complex	Molar extinction coefficient [$M^{-1}cm^{-1}$]	(%) Hypochromicity	Red shift [nm]	K [$M^{-1}cm^{-1}$][a]
1[b]	16000	49.0	5	1.00×10^4
2[c]	25626	34.8	11	1.65×10^5
3[d]	20134	41.8	16	2.80×10^5

[a] Error **2** $=3.11\times10^4\,M^{-1}$; error **3** $=5.90\times10^4\,M^{-1}$. [b] Data previously reported by Cusumano and co-workers.[28] [c] Binding constant measured at 305 nm. [d] Binding constant measured at 302 nm.

UV/Vis binding titrations: The changes in absorbance of a DNA intercalator are commonly used to assist in the determination of its binding mode and binding affinity. The hypochromicity in the absorbance spectrum of the intercalator arises from the alteration of its electric transition dipole moment upon intercalation to DNA. Upon titration with calf-thymus DNA, complex **2** demonstrated significant hypochromicity of 34.8%, and an 8 nm red shift of the π–π* band at 305 nm (Figure 1). Complex **3** showed slightly stronger hypochromicity, 42.1%, and a greater red shift of the π–π* band at 302 nm of 16 nm. It is well documented that upon intercalation significant hypochromism, broadening, and red shift of the absorbance bands occurs.[38] Based on these previous observations, our data suggests that both complexes **2** and **3** bind to calf-thymus DNA through an intercalative mode.

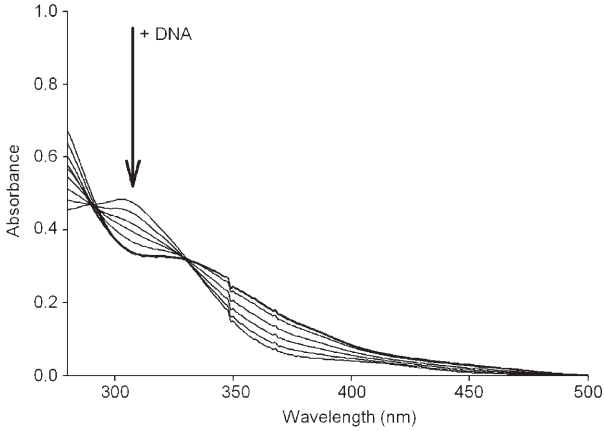

Figure 1. UV/Vis titration of complex **3** (20 μM) in phosphate buffer solution with the addition of aliquots 1 μL of calf-thymus DNA.

Binding constants, K, were determined from a reciprocal plot of $D/\Delta\varepsilon_{ap}$ versus D, using Equation (1).[34]

$$D/\Delta\varepsilon_{ap} = D/\Delta\varepsilon + 1/(\Delta\varepsilon \times K) \quad (1)$$

In Equation (1), DNA is expressed in base pairs, the apparent molar extinction coefficient $\varepsilon_A = A_{obs}/[complex]$, $\Delta\varepsilon_{ap} = |\varepsilon_A - \varepsilon_F|$ and $\Delta\varepsilon = |\varepsilon_B - \varepsilon_F|$ with ε_B and ε_F representing the molar extinction coefficients of bound Pt^{II} complex that is intercalated within the DNA duplex, and free Pt^{II} complex that is in solution, respectively. Using values obtained for the slope and the *y*-intercept from the linear fit of the reciprocal plot of $D/\Delta\varepsilon_{ap}$ versus D [Eq. (1)] was solved to give the intrinsic binding constant, K. The binding constant values are listed in Table 1.[39]

Both complexes **2** ($K=1.65\times10^5\,M^{-1}$) and **3** ($K=2.80\times10^5\,M^{-1}$) show moderate binding to calf-thymus DNA, with complex **3** showing a slightly higher binding affinity. Comparatively, the experimentally determined binding affinities are in the average range for most reported platinum metallointercalators but, are substantially lower than those observed for their ruthenium counterparts with similar π-extended ligands, such as $[Ru(dppz)(phen)_2]^{2+}$ ($K\approx10^7\,M^{-1}$).[40] Complexes **2** and **3** show higher binding affinities to duplex DNA than the large π-surface complexes, [Pt(dppz)(L)]

($K = 10^4\,\text{M}^{-1}$) studied by Che and co-workers[27] but demonstrate lower binding affinity than small π-surface Pt^{II} complexes such as [Pt(4,4′-phenyl-2,2′-bipyridine)] ($K = 10^6\,\text{M}^{-1}$).[41] As mentioned earlier, this data suggests that the large π-surface of many platinum intercalators, such as **2** and **3**, is potentially less suitable for binding to duplex DNA and a more favorable target may be the larger π-surface of the guanine quartet.

Thermal denaturation studies: Stabilization of the duplex structure through DNA intercalation is usually reflected in a significant increase of the DNA melting temperature. Thermal denaturation of calf-thymus DNA was performed with several different DNA binders, including ethidium bromide, complexes **1**–**3**, in a low ionic strength phosphate buffer. The T_m for calf-thymus DNA without any of the intercalators was 57.4 °C. Upon addition of any of the above DNA intercalators, an increase in the melting temperature of calf-thymus DNA was observed. Ethidium bromide demonstrated the lowest increase of 6.2 °C and complex **2** showed the greatest T_m increase of 15.7 °C (Table 2). Interestingly, the T_m of DNA with complex **3** is less than that of complex **2**, and this could be explained by a perturbation of the duplex structure upon intercalation of the bulkier naphthyl ligand. Both complexes **2** and **3** increase the melting temperature of DNA by more than 10 °C, consistent with the behavior of previously reported DNA intercalators. Thus, the binding mode of these complexes is most likely through intercalation.

Table 2. Average T_m and ΔT_m for CT-DNA (78 μM) in 1 mM NaH_2PO_4/Na_2HPO_4 and 2 mM NaCl, in the presence of various DNA intercalators (7.8 μM).

	T_m [°C]	ΔT_m [°C]
calf-thymus DNA	57.4	–
ethidium bromide	63.6	6.2
1	68.1	10.7
2	73.1	15.7
3	71.0	13.6

Under the experimental conditions used, biphasic behavior was observed in all intercalator/DNA thermal denaturation profiles, with complex **3** demonstrating this effect most strongly. As a result, it was challenging to obtain accurate melting temperature data from first derivative curves. Instead, an average melting temperature was estimated through determination of the average of the melting profiles within the biphasic curves. This biphasic behavior has been reported previously with other DNA intercalators[42] and most likely results from their non-homogeneous, sequence-selective aggregation along the duplex. This mode of aggregation would give rise to two observable transitions, a first melting transition resulting from the fraction of the duplex that does not contain the intercalator and a second transition arising from the segment of DNA containing the intercalator.

CD studies: Circular dichroism spectra can provide insight into the orientation of a DNA binder within the duplex. Upon binding to B-DNA, a circular dichroic peak can be induced in an achiral DNA binder through either perturbation of its molecular geometry or through electric or magnetic interactions with the duplex. Based on the magnitude and sign of the induced circular dichroic (ICD) peaks, groove binding or intercalative interactions can be inferred. Typically, groove binding[43] molecules show strong positive ICD peaks arising from transition moments aligned along the groove, whereas intercalators[44] show weaker positive or negative signals.

CD spectra were recorded with calf-thymus DNA using a 1:10 ratio (intercalator to DNA in base pairs) at room temperature. Low drug binding ratios and ionic concentrations were used so that ICD spectra observed are due to DNA interactions and not to interactions amongst aggregated chromophores. Typically, ICD spectra are observed in the region of 300–500 nm so as not to overlap with DNA. However, most of the π–π* transitions of complexes **1**, **2**, and **3** in the UV spectrum are slightly above 300 nm and thus, are close to the region where the DNA signature is observed. As a result, to obtain the ICD spectrum, CD spectra of the DNA duplex were subtracted from those containing the DNA binder (Figure 2).

A positive ICD signal was observed in the CD spectrum of **1** with calf-thymus DNA at 309 nm. The location of this signal is in agreement with the peak observed in the 300 nm region of the absorbance spectrum of **1** without any DNA present. Both complexes **2** and **3** show weakly positive ICD signals in the regions of their red-shifted π–π* ligand-centered transitions in the UV/Vis titrations with DNA, at 312 and 316 nm respectively (Figure 2). Moreover, additional weakly positive signals are observed for both complexes in the region of 425 nm, which are attributed to the MLCT bands of the complexes, as observed in the UV/Vis spectra. The presence of weak ICD signals in the CD spectra for all Pt^{II} complexes tested, upon addition of DNA, is indicative

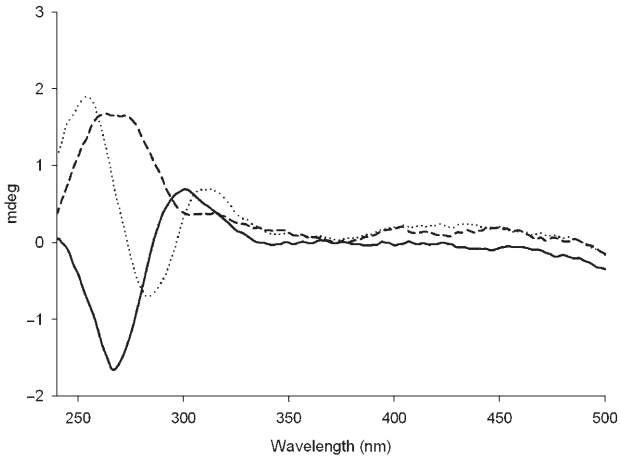

Figure 2. ICD spectra of Pt^{II} intercalators (10 μM) with calf-thymus DNA (100 μM); complex **1** (——), complex **2** (-----), and complex **3**(•••••).

of an intercalative mode of interaction with the DNA duplex.

Quadruplex binding studies: A standard 12-mer intermolecular quadruplex DNA forming sequence, ($T_4G_4T_4$), was used to evaluate the degree of interaction of the Pt^{II} complexes with this nucleic acid structure. A G-quadruplex was prepared as previously reported[22] and its structure was verified by observation of the intermolecular quadruplex DNA CD signature.

UV/Vis binding titrations: UV/Vis binding titrations were performed to determine the binding affinity of complexes **1**–**3** to the intermolecular G-quadruplex. A quadruplex DNA sample was added in aliquots sequentially to complex solutions, with absorbance spectra recorded after each addition. In the case of complex **1**, a more concentrated quadruplex DNA solution was necessary to achieve measurable binding. Ten minutes were allowed between additions to ensure that equilibrium between the Pt^{II} complexes and quadruplex DNA could be reached, and the acquisition of spectra was halted when absorbance of the peak of interest stabilized. All complexes showed hypochromicities of greater than 32%, comparable to other G-quadruplex intercalators found in the literature. Complex **1** demonstrated the smallest red shift, and complexes **2** (Figure 3) and **3** demonstrated more substantial red shifts of 7 and 16 nm, respectively (Table 3). The substantial increase in the values across the series of complexes **1**–**3** suggests strong binding to the ends of the G-quadruplex through increased π-stacking interactions as the π-surface of the complex increases.

Absorbance data collected during the titration was treated with Equation (1),[34] to give the binding constants in Table 3.[25,45] Complex **1**, which possesses the smallest π-surface, shows the lowest binding affinity to quadruplex DNA ($K = 1.75 \times 10^5\,M^{-1}$) and is on the lower end of the range of most G-quadruplex binders.[17,22,24,26] Complexes **2** and **3** demonstrate significantly stronger binding affinity to quadruplex DNA than complex **1**, with binding constants in the range of 10^6–10^7, falling in the upper range of binding affinities reported for transition-metal and organic-based quadruplex DNA binders.[17,22,24,26] All complexes tested demonstrate stronger binding to quadruplex DNA over duplex DNA by at least an order of magnitude; however, complexes **2** and **3** show the greatest preference for the quadruplex DNA structure with nearly two orders of magnitude difference in the case of complex **3**. This increase in binding affinity by the phenanthroimidazole-based Pt^{II} complexes is likely a result of a greater π-surface match between these extended complexes and the quadruplex DNA surface, and increased π–π stacking interactions and van der Waals contacts.

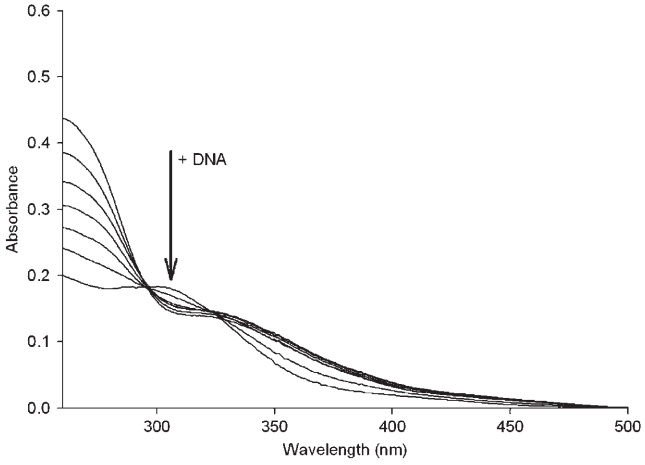

Figure 3. UV/Vis titration of complex **3** (20 μM) in phosphate buffer solution with the addition of 1 μL aliquots of G-quadruplex DNA.

Table 3. Spectral shifts and binding constants of Pt^{II} complexes upon addition of quadruplex DNA.

Complex	K [M^{-1} cm^{-1}][a]	(%) hypochromicity	Red shift [nm]
1	1.75×10^5	39.8	2
2	1.39×10^6	32.4	7
3	1.32×10^7	34.7	16

[a] Error **1** = 1.50×10^4; error **2** = 1.78×10^5; error **3** = 8.67×10^5.

Continuous variation analysis: Continuous variation analysis (Job Plot) was used to determine the binding stoichiometry of the platinum complexes with quadruplex DNA. From the intersection points obtained in the Job Plot (Figure 4), binding stoichiometries for complexes **1**, **2**, and **3** were obtained. The Pt^{II} complexes demonstrated binding stoichiometries on the order of two platinum complexes per quadruplex.

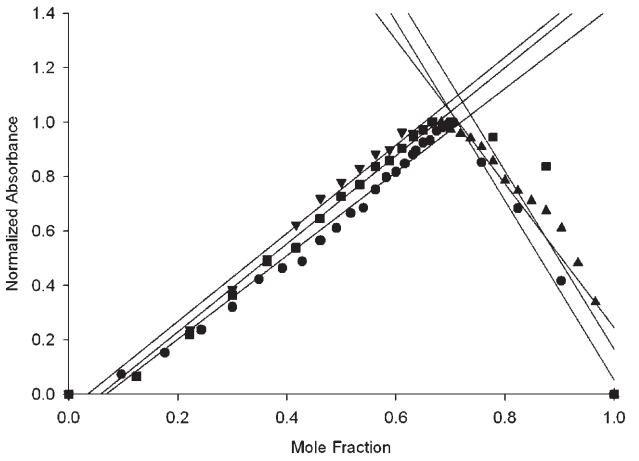

Figure 4. Job plot of Pt^{II} intercalators with quadruplex DNA, total concentration maintained between 5–10 μM; complex **1**(●), **2**(▲) and **3**(■).

For the intermolecular G-quadruplex target used in this study, the main mode of interaction is thought to occur through end-stacking, and not intercalation within the quadruplex. The observed binding stoichiometry is consistent with this mechanism, as there are two binding sites between

the ends of the guanine tetrads and the start of the thymine tetrads on both sides of the quadruplex DNA in the $T_4G_4T_4$ sequence.

CD studies: CD experiments[46] were conducted to provide insight into the stability of the G-quadruplex/Pt^{II} complexes. Samples containing G-quadruplex alone, as well as this structure with complexes **1**, **2** and **3** were prepared, and the quadruplex DNA CD signature was recorded at 240 and 260 nm.[47] A slight decrease at 260 nm and a slight increase at 240 nm in the CD signature of the intermolecular quadruplex solution are observed with complexes **2** and **3** prior to heating, which likely indicates a slight perturbation of the quadruplex DNA secondary structure as a result of end-stacking (Figure 5).

Samples were then heated to 90 °C for 10 min, cooled for about 3 h, and their CD spectra were recorded again. For the quadruplex DNA without any intercalator, a red shift of the positive peak at 260 nm to 273 nm with substantial decrease in its intensity, and an increase of the negative peak with a slight blue shift at 243 nm to 249 nm are observed (Figure 6). This change in the CD signature suggests a significant disruption in the quadruplex structure, and is consistent with previous observations of slow re-association kinetics after thermal denaturation of intermolecular DNA quadruplexes.[47,48] In the samples with complex **1**, the G-quadruplex signature is only partially maintained after heating/cooling, with a slightly greater signal at 270 nm than the free quadruplex. On the other hand, in the samples containing complexes **2** or **3**, the structure of the quadruplex DNA is almost entirely maintained after heating/cooling and the magnitude of the signature is comparable to that of the quadruplex DNA and intercalator complex prior to heating. This data suggests significant stabilization of G-quadruplex structures with the phenanthroimidazole Pt^{II} complexes to a sufficient degree that thermal denaturation is inhibited, and is consistent with their strong binding affinity to this motif.

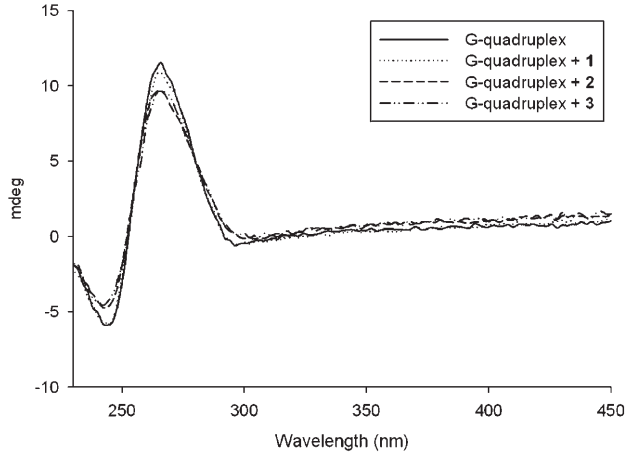

Figure 5. CD spectra of intermolecular G-quadruplex/Pt^{II} complexes prior to heating.

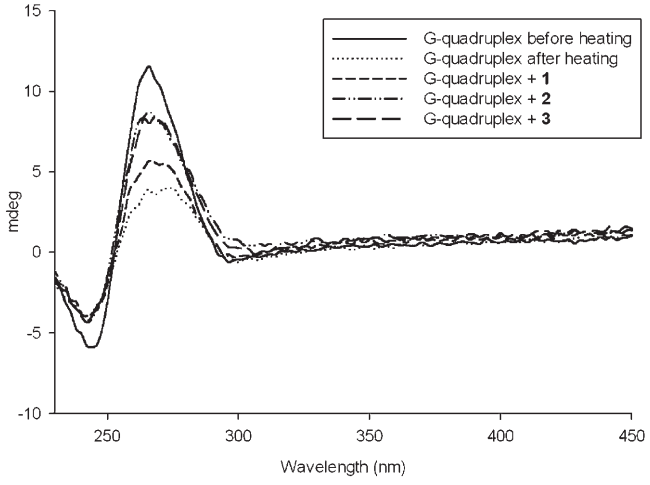

Figure 6. CD spectra of intermolecular G-quadruplex before heating and G-quadruplex with Pt^{II} complexes after heating.

Competitive dialysis: Competitive dialysis experiments were performed to evaluate the relative binding preference of Pt^{II} intercalators **1**–**3** for intermolecular quadruplex DNA versus calf-thymus duplex DNA (Figure 7).[49] Nucleic acid samples were incubated with the DNA binder (5–10 μM concentration) for 24 h.[49,50] All Pt^{II} intercalators demonstrated increased preference for quadruplex over duplex DNA, as already demonstrated with the UV/Vis studies (see above). Of note, however, is that more than a fivefold higher concentration of complex **1** was necessary to observe any UV/Vis signal for bound complexes, and the bound concentrations with both duplex and quadruplex DNA were low. This result is consistent with the lower binding affinity of this complex to the DNA structures. Complexes **2** and **3**, on the other hand, show significantly greater concentration of bound species, and dramatic preference for quadruplex over duplex DNA (34.6 μM and 49.4 μM with g-quadruplexes compared with 6.4 μM and 8.3 μM for calf-thymus DNA).

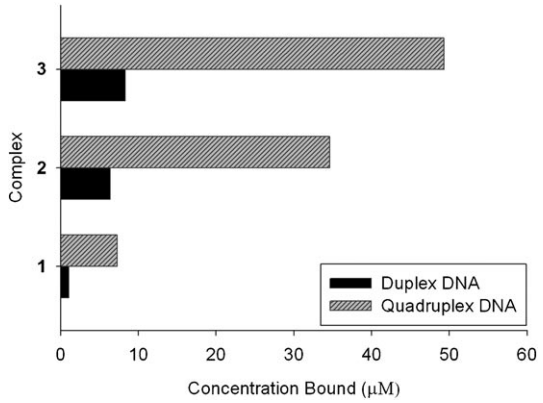

Figure 7. Competitive dialysis experiments summary; ligand concentration at 1 μM and nucleic acid concentration at 75 μM. Data was scaled to a 1 μM ligand concentration for comparison.

It is of note that while competitive dialysis is useful as a rapid tool to measure the relative binding affinity of a DNA intercalator to a large number of different nucleic acids in a single experiment, equilibrium dialysis data has been found to be less reliable than other spectroscopic methods for obtaining absolute binding constants.[49–52] Nevertheless, we were interested to test whether this method is able to reproduce the general binding trends obtained from the UV/Vis data above. Data was fitted to Equation (2), where C_b is the amount of Pt^{II} complex bound, S_{tot} is the total concentration of nucleic acid in either base pair or tetrad, and C_f is the concentration of the unbound Pt^{II} complex.

$$K_{app} = C_b/C_f{}^*(S_{tot}-C_b) \quad (2)$$

Using Equation (2), binding constants obtained for complexes **1**, **2**, and **3** to B-DNA were comparable to those obtained in UV/Vis titration experiments (Table 4). Binding constants to G-quadruplexes by the Pt^{II} intercalators were determined to be an order of magnitude higher than to B-DNA, consistent with the trends obtained from the UV/Vis titration experiments. Thus, competitive dialysis clearly shows a significant binding preference to the G-quadruplex motif over duplex DNA for complexes **2** and **3**, consistent with optimized matching of this surface with the extended π-surface of G-tetrads.

Table 4. Binding affinities for Pt^{II} complexes with calf-thymus and quadruplex DNA as determined by equilibrium dialysis experiments.

Complex	Duplex DNA K [M^{-1}]	Quadruplex DNA K [M^{-1}]
1[b]	2.72×10^4	1.11×10^5
2[c]	1.06×10^5	2.98×10^5
3[d]	1.19×10^5	7.63×10^5

Molecular modeling studies: Although challenging, molecular modeling of transition-metal complexes within the G-quadruplex structure can provide insight into the types of interactions between the DNA binder and the nucleic acid structure. In a first step, force field parameters for the metal complex were developed and a starting open structure of the G-quadruplex was prepared. This structure was constructed and refined by using a combination of molecular dynamics simulations and optimizations through energy minimization (see Experimental Section). Once the transition-metal complex and the nucleic acid structure were prepared, the metal complex was inserted into the G-quadruplex structure. In a subsequent step, a local conformational sampling was performed to optimize the G-quadruplex/DNA intercalator system. From this computational investigation, a binding mode of the platinum complex was obtained in which this complex resides between a thymine and guanine tetrad in the sequence $(T_4G_4T_4)_4$. From previous modeling studies,[18] it has been shown that the metal center of the transition-metal complex resides above the center of the G-tetrad structure. However, our modeling investigation of complexes **2** and **3** depicts a different binding picture, where the platinum atom is off-center due to the presence of three unforeseen hydrogen bonds between the ethylenediamine ligand and the DNA phosphate backbone (Figure 8). A closer look at the modeled structure also reveals a π-stacking interaction between the large aromatic system of the platinum intercalator and three guanine and thymine bases of both tetrads. Moreover, the predicted structure of the intercalator/G-quadruplex complex also indicates that most of the π-stacking interaction occurs with one thymine base (bottom right, Figure 8) and one guanine base (top left, Figure 8) in each tetrad. From this model, it is clear that truncating the aromatic system of the platinum intercalator would lead to a drop of this aromatic stacking interaction. Therefore, the predicted model suggests that a

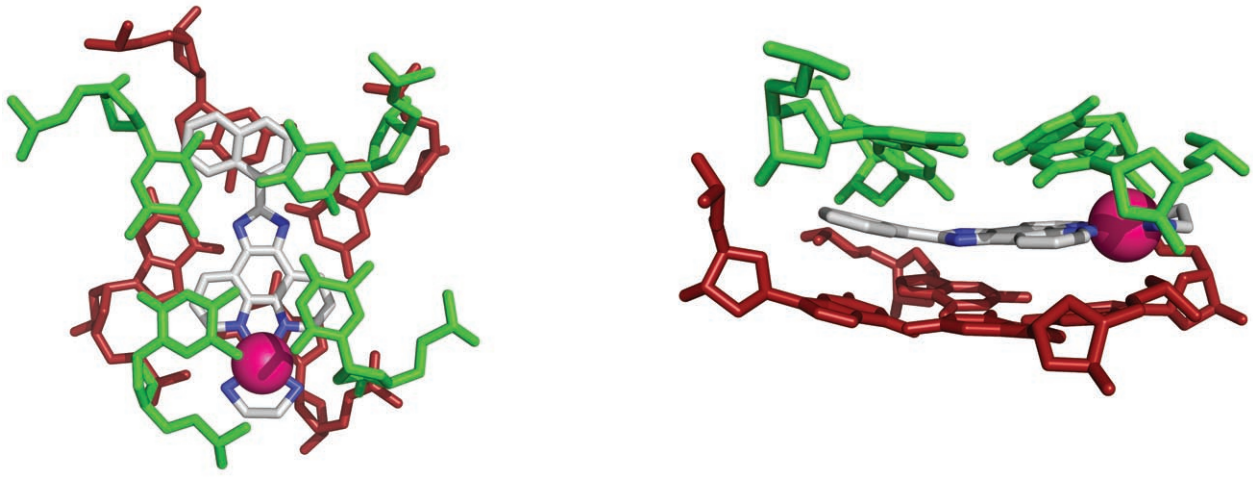

Figure 8. Predicted interaction between complex **3** and the intermolecular G-quadruplex. The platinum complex is in gray, while the G-tetrad is shown in burgundy, and the T-tetrad is in green. Hydrogen bonding between complex **3** and the G-quadruplex is depicted by the dashed lines (top view, left; side view, right). Hydrogen atoms are omitted for clarity.

greater π-surface in the G-quadruplex binder would result in higher binding affinity to this DNA motif. This model is supported by UV/Vis titration experiments with a significant increase in K observed upon the increase of the π-surface from the bipyridine to the phenanthroimidazole ligand.

Conclusion

In summary, we have reported the first synthesis, biological, and molecular modeling studies of a series of Pt^{II} intercalators with duplex and quadruplex DNA. For these studies, the small platinum molecule $[Pt(bpy)(en)]^{2+}$ (**1**), as well as a new class of more π-extended Pt^{II} phenanthroimidazole intercalators, containing phenyl (**2**) and naphthyl (**3**) substituents were synthesized. UV/Vis titration, thermal denaturation, and circular dichroism experiments show that complexes **2** and **3** bind to calf-thymus B-DNA ($\approx 10^5\,M^{-1}$) through an intercalation mechanism. Spectroscopic titration and competitive dialysis studies show significantly greater binding affinity and selectivity for quadruplex over duplex DNA structures for complexes **2** and **3**, with complex **3** displaying almost two orders of magnitude binding preference to quadruplex DNA ($\approx 10^7\,M^{-1}$). Circular dichroism experiments demonstrate that the larger Pt^{II} complexes **2** and **3** significantly increase the stability of the G-quadruplex towards thermal denaturation, while the smaller complex **1** only partially maintains the quadruplex structure after heating. Molecular modeling studies of the platinum intercalators support the preference of the phenanthroimidazole platinum intercalator for the intermolecular G-quadruplex structure through favorable π-stacking interactions, and reveal additional hydrogen bonding interactions between the ethylenediamine ancillary ligand and the phosphate backbone. Our studies thus indicate strong binding of square planar Pt^{II} intercalators to G-quadruplexes as their π-surface increases, and significant preferential binding and stabilization of quadruplex versus duplex DNA. While Pt^{II} complexes with aromatic ligands have long been studied as duplex DNA intercalators, this is the first evaluation of their potential as G-quadruplex binders. Overall, this work points to a simple method to design effective G-quadruplex binders, through combination of square planar Pt^{II} with extended aromatic ligands, to provide a π-surface that is more compatible with the larger G-quartet motif. Considering the wealth of readily obtained aromatic ligands, and the ability to easily vary the ancillary ligands on Pt^{II} complexes, this approach is amenable to rapid library creation of G-quadruplex binders of high affinity and selectivity for this motif. Future studies to determine the efficacy of these compounds to target the human quadruplex structure and inhibit telomerase are underway.

Experimental Section

Materials: All chemicals were used as received from Sigma-Aldrich without further purification for synthesis of the ligands, their respective complexes and buffer solutions. $[Pt(bpy)(en)][PF_6]_2$(**1**) was synthesized using a previously reported literature procedure.[32] Platinum complexes, once synthesized, were stored in DMSO prior to addition and added to DNA containing solutions in DMSO such that the total DMSO content was 3%.

Calf-thymus DNA was purchased from Sigma-Aldrich and dissolved overnight in a 1 mM Na_2HPO_4/NaH_2PO_4 and 20 mM NaCl solution for UV/Vis studies. For melting temperature studies calf-thymus DNA was dissolved in 1 mM Na_2HPO_4/NaH_2PO_4 and 2 mM NaCl. Calf-thymus DNA was quantified by measuring absorbance at 260 nm using the following previously determined molar extinction coefficient, $\varepsilon = 6600\,M^{-1}\,cm^{-1}$.[33] The 12-mer sequence used to generate the model quadruplex (dTTTTGGGGTTTT) was purchased from Sigma Genosys and dissolved in 10 mM K_2HPO_4/KH_2PO_4 and 49 mM KCl. Owing to the immediate hybridization of quadruplex structure under the buffer conditions, a molar extinction coefficient for the quadruplex was determined. Absorbances at 260 nm were measured for quadruplexes at 25 °C and at 90 °C. Using the molar extinction coefficient of the single stranded 12-mer; $\varepsilon = 106400\,M^{-1}\,cm^{-1}$, the concentration of the quadruplex was calculated. For competitive dialysis studies, Pierce slide-a-lyzer mini-dialysis kits (MWCO 3500 Da) were purchased from Fischer Scientific.

UV/Vis studies: Absorption spectra were recorded on a Cary 300 bio UV/Vis spectrophotometer. For UV/Vis binding measurements with calf-thymus DNA, a buffer solution of 1 mM Na_2HPO_4/NaH_2PO_4 and 20 mM NaCl was used. UV/Vis spectra were recorded after each addition of concentrated DNA solution(1 μL) in base pairs, to 10–20 μM Pt^{II} complex solutions in a 1-cm path length quartz cuvette. The same procedure was repeated with quadruplex DNA in order to obtain binding data. Binding data was then treated with Equation (1)[34] see results and discussion below.

Continuous variation analysis: Continuous variation analysis was performed according to a previously reported literature procedure.[22] Stock solutions from 5–20 μM of complexes **1**, **2**, and **3** were prepared. The corresponding quadruplex DNA solutions were made to match the concentration of the stock solutions in 10 mM K_2HPO_4/KH_2PO_4, and 49 mM KCl at pH 7.1. The total concentrations of the complex solutions were maintained at the value of the starting stock solution throughout the titrations. Wavelengths for each complex similar to those monitored in the UV/Vis titrations were used. Absorbance difference spectra were collected from 200 nm to 500 nm with quadruplex DNA at the concentration being measured as the reference. Linear regression analysis was performed in SigmaPlot for each set of data points.

Melting temperature studies: UV melting studies were also performed on the Cary 300 bio equipped with thermostatically controlled cell holder heated by a circular water bath. DNA/Pt^{II} complex solutions (10:1 ratio of DNA in base pairs to Pt^{II} complex at a concentration of 7.8 μM) were dissolved in a 1 mM Na_2HPO_4/NaH_2PO_4 and 2 mM NaCl buffer solution. These solutions were heated from 5 °C to 95 °C at a rate of 0.5 °C min^{-1} and monitored continuously at 260 nm. T_m values were determined from plots of absorbance versus temperature.

CD spectroscopy: CD spectra were recorded on a JASCO J-810 spectrophotometer. For duplex DNA experiments, samples of the DNA/Pt^{II} (10:1 ratio DNA in base pairs to Pt^{II} complex at a concentration of 10 μM)) complex were dissolved in a 1 mM Na_2HPO_4/NaH_2PO_4 and 2 mM NaCl buffer and placed in a 0.1-cm path length quartz cuvette. Each spectrum was collected from 350 nm to 220 nm at a scan speed of 100 nm min^{-1}. In addition, each spectrum collected was an average of three scans and a spectrum of the corresponding buffer were subtracted from that of the sample. A CD spectrum of calf-thymus DNA in buffer was used as a blank and then subtracted from the DNA/intercalator sample to obtain the ICD spectrum. ICD data was smoothed using the means-movement function in the JASCO graphing software.

For the quadruplex experiments, samples were dissolved in the same buffer as for the duplex experiments. Spectra were recorded under the same conditions for the duplex experiments except samples were prepared as a 1:1 ratio of quadruplex in tetrad to Pt^{II} at a concentration of 34.8 μM. Samples were heated to 95 °C for 10 min and then cooled over 2–3 h at room temperature. CD spectra were collected before and after heating at room temperature.

Competitive dialysis: A dialysis solution containing a 10 μM solution of the Pt^{II} complex (80 mL), 200x the total amount of nucleic acid to be tested, in a 1 mM NaH_2PO_4/Na_2HPO_4 and 2 mM NaCl buffer (pH 7.0) was prepared. Nucleic acids to be dialysed against the Pt^{II} complexes were prepared to be 75 μM in either base pair or base quartet in buffer (200 μL). The dialysis units were positioned slightly above the dialysis solution within the beaker and were covered with parafilm and aluminum foil. The setup was then allowed to equilibrate for 24 h with stirring at room temperature. After equilibration, the dialysis solution (180 μL) was added to a microcentrifuge tube along with a 10% (w/v) SDS solution (20 μL) to give a final concentration of 1% SDS. The SDS treated solutions and the dialysis buffer containing the Pt^{II} complex were then analyzed by UV/Vis spectroscopy after 10 min to determine the amount of intercalator present inside and outside of the dialysis bag.

Synthesis of naphthylphenanthroimidazole (PIN) ligand: The naphthyl derivatized ligand was synthesized using the procedure as outlined by Steck and Day.[35] Column conditions were modified, so the mixture was first eluted with a hexanes/ethyl acetate mixture (70:30) to remove starting material and the product was then eluted with a dichloromethane/methanol mixture (97:3). The product was then evaporated to yield an oily residue. A small amount of $CHCl_3$ was added to precipitate the product as a pale yellow solid. Yield: 29% ^{1}H NMR (500 MHz, [D$_6$]DMSO): $\delta = 9.111$ (d, 1H), 9.047(br. d, 2H), 8.958 (br. s, 2H), 8.125 (m, 2H), 8.069 (d, 1H), 7.863 (m, 2H), 7.737 (t, 1H), 7.681 (t, 1H), 7.633 ppm (t, 1H); ^{13}C NMR (300 MHz, [D$_6$]DMSO): $\delta = 123.556$, 124.092, 124.403, 125.035, 125.371, 126.119, 126.522, 127.280, 127.445, 128.094, 128.496, 130.138, 130.229, 130.691, 133.733, 135.466, 135.731, 136.789, 143.162, 147.872, 150.770, 150.771, 151.047 ppm; MS (ESI, 90 MeOH: 10 DMSO): m/z (%): calculated 346.12185, found 347.12873 ([M+1]).

Synthesis of PIPPtCl$_2$: The phenylphenanthroimidazole ligand was synthesized by using the procedure as outlined by Steck and Day.[34] K_2PtCl_4 (215 mg, 5.18 mmol) was first dissolved in DMSO (3 mL) and distilled water (1 mL) and heated to near boiling. This hot solution was added to a hot solution of phenylphenanthroimidazole (153 g, 5.18 mmol) in DMSO (5 mL). The reaction mixture was allowed to cool overnight and then vacuum-filtered. The yellow dichloride product was washed with water to remove excess K_2PtCl_4, a small amount of ethanol, and diethyl ether to dry the product. Yield: 79% ^{1}H NMR (300 MHz, [D$_6$]DMSO): $\delta = 9.657$ (d, 2H), 9.289 (d, 2H), 8.293 (d, 2H), 8.223 (t, 2H), 7.613 ppm (m, 3H); MS (ESI, CH_3CN and NaI): m/z (%): calculated 561.00868, found 582.99579 ([M^++Na$^+$]) with ^{194}Pt.

Synthesis of PINPtCl$_2$: The same procedure was used as for the synthesis of PIPPtCl$_2$, except (102 mg, 0.294 mmol) of the naphthylphenanthroimidazole ligand and (122 mg, 0.294 mmol) of K_2PtCl_4 were used. Yield: 82% ^{1}H NMR (500 MHz, [D$_6$]DMSO): $\delta = 9.613$ (d, 2H), 9.294 (d, 2H), 9.068 (d, 1H), 8.166 (4H), 8.105 (d, 1H), 7.778 (t, 1H), 7.683 ppm (m, 2H); MS (ESI, CH_3CN and NaI): m/z (%): calculated 611.02433, found 634.01243 ([M^++Na$^+$]) with ^{194}Pt.

Synthesis of [(PIP)Pt(en)][PF$_6$]$_2$ (2): Ethylenediamine (106 μL, 1.57 mmol) was added to a suspension of (PIP)PtCl$_2$ (88.5 mg, 0.157 mmol) in ethanol (20 mL). The reaction mixture was refluxed for 3 h and a small amount of distilled water was added to the reaction mixture until the solution turned a clear red color. The reaction mixture was then gravity filtered to remove any unreacted material, and ammonium hexafluorophosphate was added to precipitate the off-yellow product. The product was filtered on a glass frit and washed with a small amount of ethanol and diethyl ether. Yield: 62% ^{1}H NMR (500 MHz, [D$_6$]DMSO): $\delta = 9.224$ (d, 2H), 9.055 (br s, 2H), 8.302, (br s, 2H), 8.247 (d, 2H), 7.662 (br s, 2H), 7.616 (d, 1H), 6.920 (br s, 4H), 2.779 ppm (br s, 4H); ^{13}C NMR (500 MHz, [D$_6$]DMSO): $\delta = 47.215$, 126.497, 129.107, 129.307, 130.649, 134.576, 144.494, 149.653, 153.082 ppm; MS (ESI, CH_3CN, trace of H_2O and formic acid): m/z (%): calculated [M−2PF$_6$]$^{2+}$ 275.56986, found 275.56913 with ^{195}Pt.

Synthesis of [(PIN)Pt(en)][PF$_6$]$_2$ (3): Complex **3** was prepared in the same manner as complex **2** except (PIN)PtCl$_2$ (69.8 μL, 0.098 mmol) and ethylenediamine (60.1 mg, 0.98 mmol) was used. Yield: 65% ^{1}H NMR (500 MHz, [D$_6$]DMSO): $\delta = 9.455$ (dd, 2H), 9.082 (d, 2H), 9.080 (m, 1H), 8.324 (dd, 2H), 8.211 (d, 1H), 8.157 (d, 1H), 8.123 (d, 1H), 717.796 (t, 1H), 7.692 (m 2H), 6.936 (br s, 4H), 2.804 ppm (br s, 4H); ^{13}C NMR (300 MHz, [D$_6$]DMSO): $\delta = 47.251$, 125.332, 125.775, 126.333, 126.455, 126.606, 127.359, 128.348, 128.658, 130.102, 130.879, 133.526, 134.667, 144.378, 149.604, 152.997 ppm; MS (ESI, CH_3CN, trace of H_2O and formic acid): m/z (%): calculated [M−2PF$_6$]$^{2+}$ 300.577685, found 300.57691 with ^{195}Pt.

Molecular modeling of the quadruplex/Pt complex system: The initial quadruplex structure was constructed from the reported NMR structure of a quadruplex DNA made of four DNA (5′-D(*TP*TP*GP*GP*GP*GP*T)-3′) units (PDB code: 139D). Two layers of thymines were added on the 5′-end using InsightII as a graphical interface to more accurately represent the experimental system. Subsequently, the Pt^{II} complexes were constructed and optimized through B3LYP density functional theory computations at the B3LYP/LACV3P* level of theory. Specific Pt^{II} force field parameters were developed from single-point DFT computations of various distorted structures of the Pt^{II} complex at the B3LYP/LACV3P**+ level of theory. LACV3P**+ is a triple-ζ basis set with polarization and diffuse functions on all atoms except hydrogens. The standard triple-zeta 6–31G basis set is used for all light elements and the Los Alamos non-relativistic effective core potential was used for Pt^{II}. All DFT computations were performed using the Jaguar7.0 program package. The developed force field parameters were incorporated into the Generalized Amber Force Field (GAFF). The platinum complex atomic partial charges were derived from the atomic electrostatic potential.

Construction and refinement of the DNA/Pt complex system: Manual intercalation of the platinum complex within the homologated quadruplex was initially performed. Three potassium ions were added in the central channel between each of the G-tetrads,[3] and the resulting system was neutralized by addition of 27 K^+ ions. These ions were added at the most negative locations as computed by the leap program and an additional 5 KCl molecules were added to simulate the ionic medium. After the addition of K^+ ions, a periodic truncated octahedron box of water was added corresponding to 10068 TIP3P water molecules. Stepwise relaxation was then performed with the slow relaxation of the entire system commencing with the water molecules. In a subsequent step, the entire system was fully minimized by using large constraints on the DNA heavy atoms and iterated through the gradual decrease of constraints on these atoms. For this purpose, the Sander program within the AMBER8.0 suite of programs was used with a combination of the parm99 force field for the G-quadruplex and GAFF for the Pt^{II} complex. A combination of 5000 steps of conjugate gradients minimization and 10000 steps of molecular dynamics at gradually increasing temperatures was used to relieve strain within the system This minimization/MD simulation procedure was iterated five times at 100 K, eight times at 200 K, and ten times at 300 K, with the use of Berendsen temperature-coupling algorithm and the SHAKE algorithm for all hydrogen atoms with 1 fs time steps. A cutoff of 11 Å was used for the computation of the van der Waals and electrostatic interactions. As these systems are highly charged, the long-range electrostatic interactions should be carefully computed. The Particle Mesh Ewald summation term was enabled with the automatically defined parameters. To maintain the integrity of the quadruplex, constraints were added on the hydrogen bond network.

Acknowledgements

This work was supported by NSERC, the Canada Foundation for Innovation, Nanoquebec, Research Corporation, Center for Self-Assembled

Chemical Structures, the Canadian Institute for Advanced Research and the NSERC Idea to Innovation program. We would like to acknowledge Dr. Gonzalo Cosa for the numerous helpful discussions and advice. We would also like to acknowledge Pablo Englebienne for assistance with modeling of Pt^{II} complexes. H. F. Sleiman is a Cottrell Scholar of the Research Corporation.

[1] M. A. Blasco, *Nat. Rev. Genet.* **2005**, *6*, 611.
[2] J. T. Davis, *Angew. Chem.* **2004**, *116*, 684; *Angew. Chem. Int. Ed.* **2004**, *43*, 668.
[3] G. N. Parkinson, M. P. H. Lee, S. Neidle, *Nature* **2002**, *417*, 876.
[4] Y. Wang, D. J. Patel, *Structure* **1993**, *1*, 263.
[5] E. H. Blackburn, *Cell* **2001**, *106*, 661.
[6] N. W. Kim, M. A. Piatyszek, K. R. Prowse, C. B. Harley, M. D. West, P. L. C. Ho, G. M. Coviello, W. E. Wright, S. L. Weinrich, J. W. Shay, *Science* **1994**, *266*, 2011.
[7] A. E. Pitts, D. R. Corey, *Proc. Natl. Acad. Sci. USA* **1998**, *95*, 11549.
[8] J. C. Norton, M. A. Piatyszek, W. E. Wright, J. W. Shay, D. R. Corey, *Nat. Biotechnol.* **1996**, *14*, 615.
[9] Y. Yokoyama, Y. Takahashi, A. Shinohara, Z. Lian, X. Wan, K. Niwa, T. Tamaya, *Cancer Res.* **1998**, *58*, 5406.
[10] M. P. Horvath, V. L. Schweiker, J. M. Bevilacqua, J. A. Ruggles, S. C. Schultz, *Cell* **1998**, *95*, 963.
[11] C. M. Price, T. R. Cech, *Genes Dev.* **1987**, *1*, 783.
[12] S. J. Froelich-Ammon, B. A. Dickinson, J. M. Bevilacqua, S. C. Schultz, T. R. Cech, *Genes Dev.* **1998**, *12*, 1504.
[13] M. Y. Kim, H. Vankayalapati, K. Shin-Ya, K. Wierzba, L. H. Hurley, *J. Am. Chem. Soc.* **2002**, *124*, 2098.
[14] G. Pennarun, C. Granotier, L. R. Gauthier, D. Gomez, F. Hoffschir, E. Mandine, J. F. Riou, J. L. Mergny, P. Mailliet, F. D. Boussin, *Oncogene* **2005**, *24*, 2917.
[15] A. M. Burger, F. Dai, C. M. Schultes, A. P. Reszka, M. J. Moore, J. A. Double, S. Neidle, *Cancer Res.* **2005**, *65*, 1489.
[16] S. M. Haider, G. N. Parkinson, S. Neidle, *J. Mol. Biol.* **2003**, *326*, 117.
[17] M. Read, R. J. Harrison, B. Romagnoli, F. A. Tanious, S. H. Gowan, A. P. Reszka, W. D. Wilson, L. R. Kelland, S. Neidle, *Proc. Natl. Acad. Sci. USA* **2001**, *98*, 4844.
[18] J. E. Reed, A. A. Arnal, S. Neidle, R. Vilar, *J. Am. Chem. Soc.* **2006**, *128*, 5992.
[19] R. J. Harrison, S. M. Gowan, L. R. Kelland, S. Neidle, *Bioorg. Med. Chem. Lett.* **1999**, *9*, 2463.
[20] D. Sun, B. Thompson, B. E. Cathers, M. Salazar, S. M. Kerwin, J. O. Trent, T. C. Jenkins, S. Neidle, L. H. Hurley, *J. Med. Chem.* **1997**, *40*, 2113.
[21] R. T. Wheelhouse, D. Sun, H. Han, F. X. Han, L. H. Hurley, *J. Am. Chem. Soc.* **1998**, *120*, 3261.
[22] R. Keating Loryn, A. Szalai Veronika, *Biochemistry* **2004**, *43*, 15891.
[23] I. M. Dixon, F. Lopez, A. M. Tejera, J. P. Esteve, M. A. Blasco, G. Pratviel, B. Meunier, *J. Am. Chem. Soc.* **2007**, *129*, 1502.
[24] I. M. Dixon, F. Lopez, J. P. Estéve, A. M. Tejera, M. A. Blasco, G. Pratviel, B. Meunier, *ChemBioChem* **2005**, *6*, 123.
[25] A. Maraval, S. Franco, C. Vialas, G. Pratviel, M. A. Blasco, B. Meunier, *Org. Biomol. Chem.* **2003**, *1*, 921.
[26] C. Rajput, R. Rutkaite, L. Swanson, I. Haq, J. A. Thomas, *Chem. Eur. J.* **2006**, *12*, 4611.
[27] C. M. Che, M. Yang, K. H. Wong, H. L. Chan, W. Lam, *Chem. Eur. J.* **1999**, *5*, 3350.
[28] M. Cusumano, A. Giannetto, *J. Inorg. Biochem.* **1997**, *65*, 137.
[29] M. Cusumano, M. L. Di Pietro, A. Giannetto, *Inorg. Chem.* **1999**, *38*, 1754.
[30] A. E. Friedman, J. C. Chambron, J. P. Sauvage, N. J. Turro, J. K. Barton, *J. Am. Chem. Soc.* **1990**, *112*, 4960.
[31] M. Cusumano, M. L. Di Pietro, A. Giannetto, *Inorg. Chem.* **2006**, *45*, 230.
[32] L. E. Erickson, *J. Am. Chem. Soc.* **1969**, *91*, 6284.
[33] G. Cosa, K. S. Focsaneanu, J. R. N. McLean, J. P. McNamee, J. C. Scaiano, *Photochem. Photobiol.* **2001**, *73*, 585.
[34] A. Wolfe, G. H. Shimer Jr, T. Meehan, *Biochemistry* **1987**, *26*, 6392.
[35] E. A. Steck, A. R. Day, *J. Am. Chem. Soc.* **1943**, *65*, 452.
[36] L. Bu, T. Sawada, H. Shosenji, K. Yoshida, S. Mataka, *Dyes Pigm.* **2003**, *57*, 181.
[37] Upon the addition of an excess of calf-thymus DNA, a slight increase in fluorescence of the Pt^{II} complex was observed but, this difference was too low for further measurements.
[38] W. I. Sundquist, S. J. Lippard, *Coord. Chem. Rev.* **1990**, *100*, 293.
[39] UV/Vis absorption curves along with plots of $D/\Delta\varepsilon ap$ versus D for complexes other than complex **3** can be found in the Supporting Information.
[40] C. Hiort, P. Lincoln, B. Nordén, *J. Am. Chem. Soc.* **1993**, *115*, 3448.
[41] M. Cusumano, M. L. Di Pietro, A. Giannetto, F. Nicolo, E. Rotondo, *Inorg. Chem.* **1998**, *37*, 563.
[42] J. B. Chaires, N. Dattagupta, D. M. Crothers, *Biochemistry* **1982**, *21*, 3933.
[43] M. Kubista, B. Aakerman, B. Norden, *J. Phys. Chem.* **1988**, *92*, 2352.
[44] B. Norden, F. Tjerneld, *Biopolymers* **1982**, *21*, 1713.
[45] Multiple binding treatments were attempted and Equation (1) provided the best fits to the data obtained. Additionally, SPR was attempted as a method to obtain binding constants but, high non-specific binding of these transition-metal complexes was observed.
[46] CD experiments were used in place of melting temperature experiments, as results from UV/Vis spectroscopy were difficult to interpret due to the absence of a true melting curve. This absence could be as a result of the high ionic strength of the buffer used to generate the quadruplex, which would prevent its denaturation although diluted for thermal denaturation experiments.
[47] J. L. Mergny, A. T. Phan, L. Lacroix, *FEBS Lett.* **1998**, *435*, 74.
[48] J. L. Mergny, A. De Cian, A. Ghelab, B. Sacca, L. Lacroix, *Nucleic Acids Res.* **2005**, *33*, 81.
[49] J. Ren, J. B. Chaires, *Biochemistry* **1999**, *38*, 16067.
[50] J. Ren, J. B. Chaires, *Methods Enzymol.* **2001**, *340*, 99.
[51] J. B. Chaires, *Top. Curr. Chem.* **2005**, *253*, 33.
[52] F. Rosu, E. De Pauw, L. Guittat, P. Alberti, L. Lacroix, P. Mailliet, J. F. Riou, J. L. Mergny, *Biochemistry* **2003**, *42*, 10361.

Received: May 24, 2007
Published online: November 19, 2007

